BC Bioconjugate Chemistry

pubs.acs.org/bc June 2018 Volume 29, Number 6

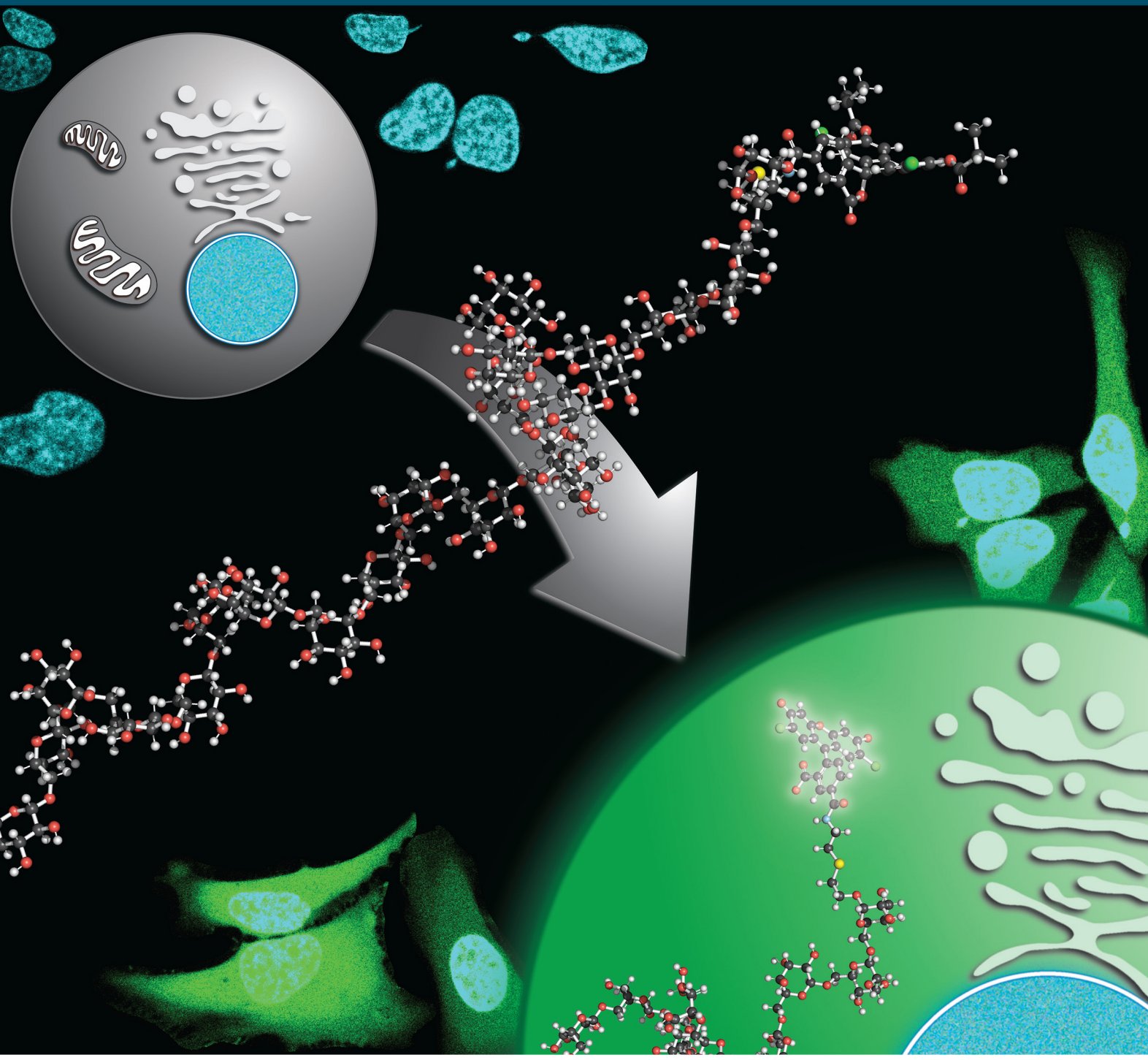

ACS Publications
Most Trusted. Most Cited. Most Read.

www.acs.org

Bioconjugate Chemistry

Article

Cite This: Bioconjugate Chem. 2018, 29, 1942−1949

pubs.acs.org/bc

Cytosolic Uptake of Large Monofunctionalized Dextrans

Wen Chyan,[†,‡,#] Henry R. Kilgore,[§,‡,#] and Ronald T. Raines*[,†,⊥,‡]

[†]Department of Chemistry, [§]Graduate Program in Biophysics, and [⊥]Department of Biochemistry, University of Wisconsin−Madison, Madison, Wisconsin 53706, United States

[‡]Department of Chemistry, Massachusetts Institute of Technology, 77 Massachusetts Avenue, Cambridge, Massachusetts 02139, United States

Supporting Information

ABSTRACT: Dextrans are a versatile class of polysaccharides with applications that span medicine, cell biology, food science, and consumer goods. Here, we report on a new type of large monofunctionalized dextran that exhibits unusual properties: efficient cytosolic and nuclear uptake. This dextran permeates various human cell types without the use of transfection agents, electroporation, or membrane perturbation. Cellular uptake occurs primarily through active transport via receptor-mediated processes. These monofunctionalized dextrans could serve as intracellular delivery platforms for drugs or other cargos.

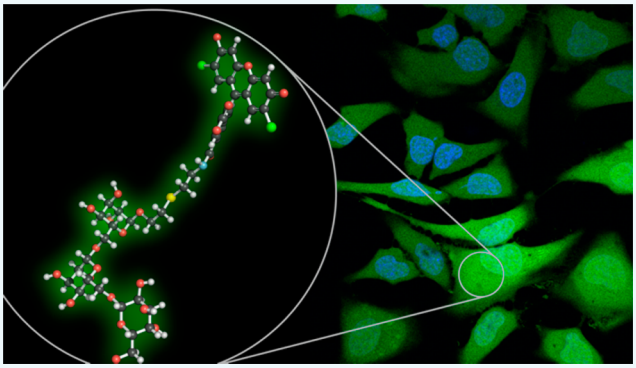

INTRODUCTION

Dextrans are glucose polymers with widespread applications in the modern clinic, laboratory, and home. Dextrans are isolated from Lactobacillales, an order of Gram-positive, low guanine−cytosine content, nonsporulating bacteria.[1] The constituent glucose units are linked through $\alpha(1,6)$-glycosidic bonds, with occasional $\alpha(1,4)$ and $\alpha(1,3)$-glyosidic linkages being introduced by biosynthetic promiscuity.[2]

Many applications of dextrans leverage its nonimmunogenic nature, large size, and viscogenic properties.[3,4] For example, dextrans are on the World Health Organization's "Model List of Essential Medicines" due to their antithrombotic and volume-expanding properties, among other beneficial effects.[5,6] Recently, dextran nanoparticles have been used as the basis for a small-molecule drug delivery platform.[7] Immediately after uptake via endocytosis, these nanoparticles degrade, allowing embedded small molecules to escape and diffuse into the cytosol.[8] In the laboratory, fluorophore-conjugated dextrans serve as a tracking agent for macro- and micropinocytosis, facilitating imaging of endocytosed particles or organisms and probing the details of autophagy.[9−11] At home, dextrans are employed as thickening agents in cuisines and as a base for cosmetics.[12,13]

To provide a conjugation handle for fluorophores or other moieties, dextrans are functionalized by either chemoselective reactions at the reducing-end[14] or nonselective reactions such as periodate oxidation.[15−17] Commercial fluorophore-conjugated dextrans are typically produced using nonspecific functionalization followed by fluorophore conjugation that peppers the dextran with up to 130 mol equiv of dye.[18] Because typical dyes are hydrophobic and interact with lipids,[19] functionalizing dextrans with excess dye risks undesirable changes to structural and surface properties. In addition, the nonselective processes that are used to polyfunctionalize dextrans can impart structural damage and leave residual reactive moieties.[20]

To overcome the limitations of current fluorophore−dextran conjugates, we sought to create a fluorogenic dextran with minimal perturbation to the dextran by selectively conjugating a fluorogenic probe to the reducing end. We chose to use a pH-independent, electronically stabilized fluorogenic probe[21] that is suitable for the next generation of agents to track endocytosis and autophagy. The probe has ester moieties that mask a fluorescent signal until entry into cells, upon which intracellular esterases cleave the masking groups and restore fluorescence. Conjugation of the probe to dextrans enables precise spatiotemporal monitoring of cellular uptake. More importantly, this fluorogenic dextran exhibits high contrast ratios and real-time imaging capabilities. These advantages stem from the fluorogenic nature of the probe, which ensures little-to-no background, even without washing of the cells. In contrast, commercially available fluorescent dextrans are constitutively fluorescent and are not amenable to real-time imaging. Finally, we compare the cellular uptake of a monofunctionalized dextran with that of polyfunctionalized dextrans. The results revealed unanticipated differences between these two types of dextrans, which suggest potential applications of monofunctionalized dextrans as a cytosolic delivery platform.

Received: March 16, 2018
Published: April 12, 2018

DOI: 10.1021/acs.bioconjchem.8b00198
Bioconjugate Chem. 2018, 29, 1942−1949

Scheme 1. (A) Synthetic Route to Conjugates 2, 3a, and 3b from Commercial Dextrans D1 and D3. (B) In Cellulo Enzymatic Activation of Conjugate 2

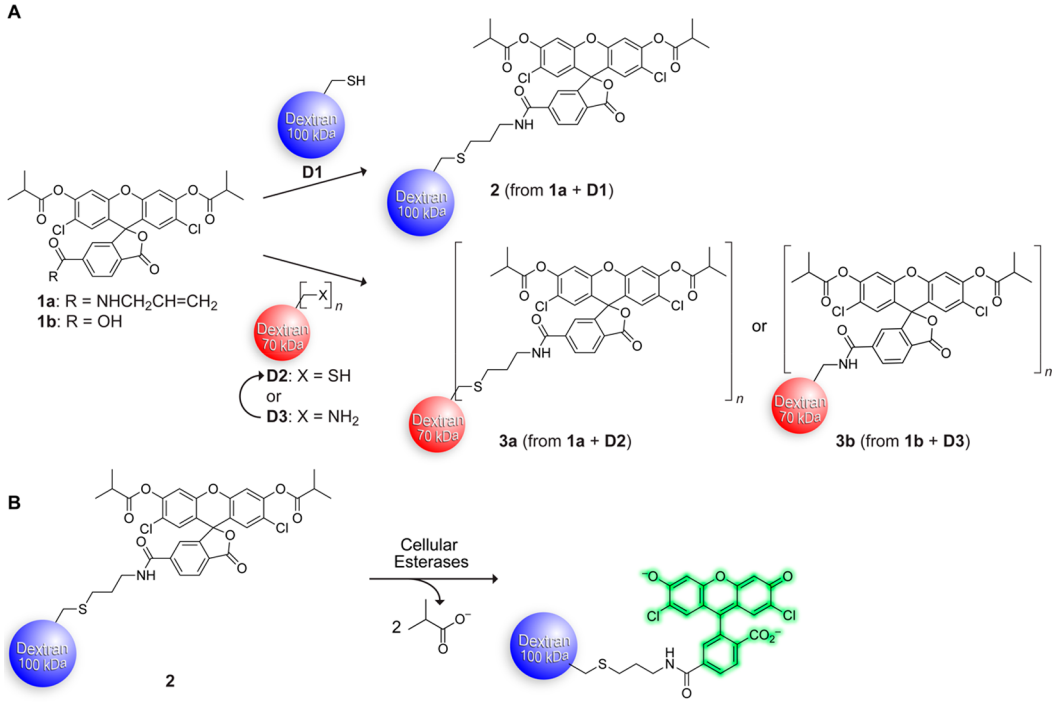

RESULTS AND DISCUSSION

Our fluorogenic probe (**1a**) was conjugated to commercial 100 kDa and 70 kDa dextrans via thiol−ene and *N*-hydroxysuccinimide-amine chemistry (Scheme 1A) to produce fluorogenic dextrans **2**, **3a**, and **3b**.[22,23] To the best of our knowledge, conjugate **2** is the first monofunctionalized fluorogenic dextran. Conjugate **2** was prepared in good yield with no residual unconjugated small molecule fluorophore contaminants. Upon incubation with pig liver esterases or upon exposure to cytosolic esterases, the isobutyryl masking groups in conjugate **2** were cleaved to effect total reclamation of fluorescence (Scheme 1B, Figure S1).

Next, we assessed the cellular uptake of conjugate **2** in HeLa cells by confocal microscopy. To our surprise, we observed the fluorescent signal for conjugate **2** to be dispersed evenly throughout the cytosol and nucleus (Figures 1A and S2−S5), instead of the punctate staining that is typical of commercially available fluorophore−dextran conjugates.[24,25] Although mixed cytosolic and vesicular uptake of dextrans was reported in a few studies using smaller polyfunctionalized dextrans,[26−28] conjugate **2** seemed to far surpass these in the efficacy of its cytosolic internalization, with no observable vesicular fluorescence.

We sought to validate our initial observations. The cytosolic dispersion of conjugate **2** was replicated consistently across different dextran batches and HeLa cell passages. Further, the same transport localization observed in HeLa cells (cervix adenocarcinoma) was observed in H1299 and H460 cell lines (non-small cell lung carcinoma), suggesting that probe entry into the cell was not an artifact of cell type (Figure 1B and C). Indeed, conjugate **2** dispersed generally throughout the cytosol and nucleus with only small deviations in rate of uptake between these three cell types (Figure 1). Imaging analysis indicates that the same linear rate function is observed in all cell types, suggesting that the mechanism of cell entry is conserved within this set.

Having established the consistent cytosolic entry of conjugate **2** into mammalian cells, we next compared conjugate **2** with commercially available fluorophore−dextran conjugates. Although conjugate **2** displayed a dispersed signal within cells (Figure 1), commercial polyfunctionalized tetramethylrhodamine−dextran conjugates of various sizes (TAMRA−dextran) showed punctate staining (Figure S6).

To ensure that the hydrophobic fluorophore-masking group and linker components of conjugate **2** did not alter the cell-penetrating properties of the dextran significantly, we also prepared polyfunctional conjugates **3a** and **3b** (Scheme 1). Although **3a** and **3b** were labeled with the same probe moiety via thiol−ene or NHS-ester chemistry, respectively, both failed to reproduce the diffuse staining achieved by conjugate **2**. Upon incubation of probes **3a** and **3b** with HeLa cells over 30 min, polyfunctionalized conjugates **3a** and **3b** behaved similarly to TAMRA−dextrans, yielding highly punctate staining patterns indicative of being trapped within endocytic vesicles (Figures S6 and S7). Accordingly, we concluded that the fluorogenic probe does not perturb dextran transport. Similarly, having either a thioether or an amide in the linker had no effect on cytosolic penetration properties, as conjugates **3a** and **3b** showed similar cellular distributions. Further, conjugate **2** exhibited increased fluorescence signal relative to conjugates **3a** and **3b**, indicating significantly higher uptake in consideration of the higher degree of dye labeling in **3a** and **3b** (Figure S8). To confirm the dextran localization patterns quantitatively, Pearson's correlation coefficients between each dextran and Lysotracker (which is a stain for acidified vesicles), or Hoechst 33342 (which is a stain for nuclei) were calculated from cell images ($n \geq 20$, Table S1). The correlation coefficients confirmed that conjugate **2** was indeed distributed throughout

DOI: 10.1021/acs.bioconjchem.8b00198
Bioconjugate Chem. 2018, 29, 1942−1949

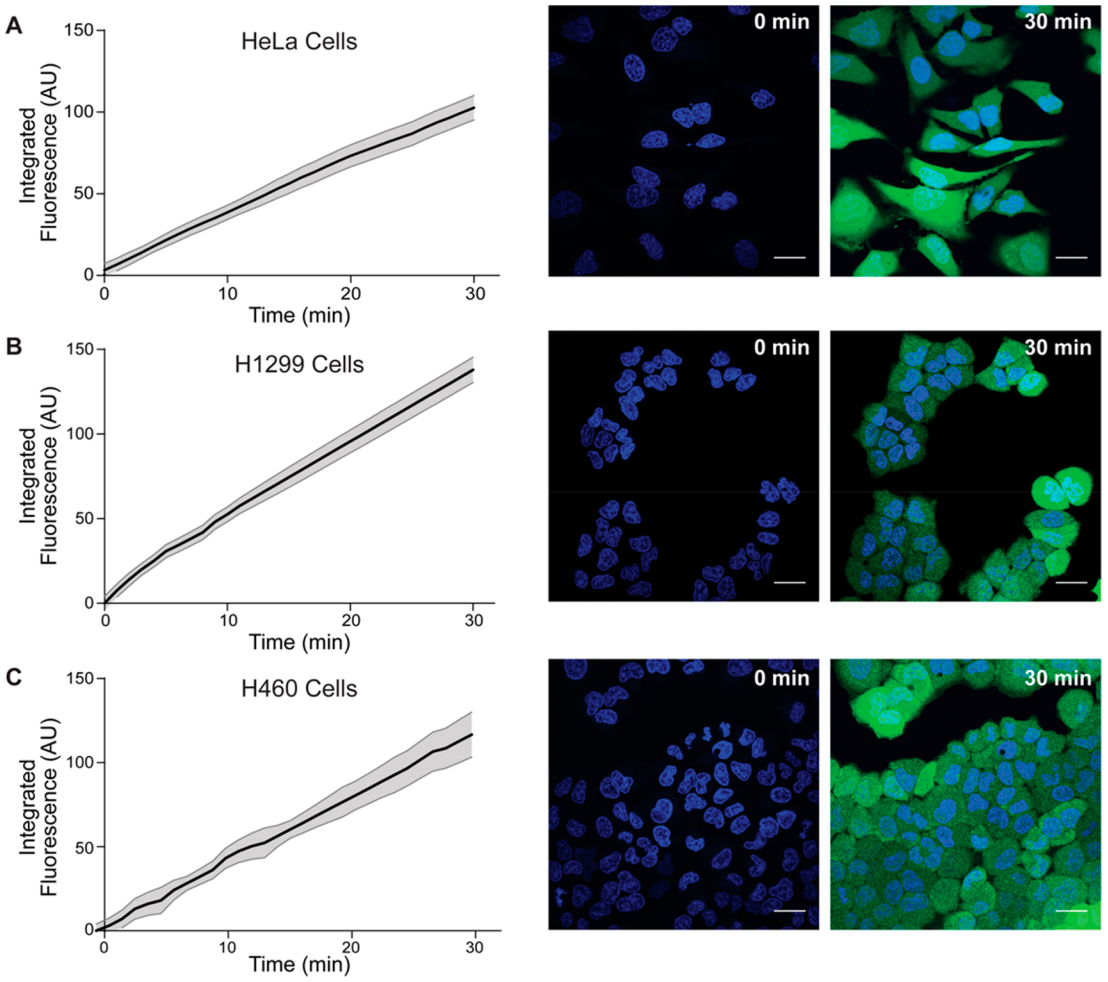

Figure 1. Uptake of conjugate **2** by human cells. Time-courses for the uptake of conjugate **2** (10 μM, green signal) were obtained by summing the background-subtracted signal within HeLa cells (A), H1299 cells (B), and H460 cells (C), counterstained with Hoechst 33342 stain (blue signal) for 15 min prior to imaging. Confocal microscopy was used to image the cells continuously from 0 to 30 min. Scale bars: 25 μm.

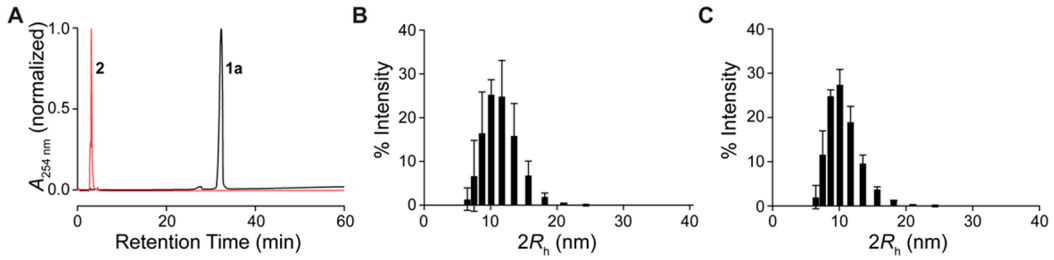

Figure 2. Graphs showing the acid stability of components of conjugate **2** upon incubation in 1.0 M HCl for 1 h. (A) C4 HPLC trace of conjugate **2** and, for reference, probe **1a**. Size distribution as measured by DLS before (B) and after (C) incubation in acid.

the cytosol whereas conjugates **3a** and **3b** correlated strongly to only the Lysotracker vesicle stain.

Next, we assessed the chemical stability of the linkers and dextran in conjugate **2**. If any of the linker components were to decompose, then the ensuing fluorescent fragments could diffuse across a lipid bilayer into the cytosol. We were concerned, for example, about acid-catalyzed hydrolysis following endocytosis. As endocytic vesicles mature, their pH drops to 4.6.[29,30] We were also concerned about enzyme-catalyzed hydrolysis, because endosomes contain glycohydrolases.[31] To test stability, we subjected conjugate **2** to conditions at least as harsh as those encountered on the route to the cytosol. After treatment, we assessed its integrity by high-performance liquid chromatography (HPLC) and dynamic light scattering (DLS). In HPLC experiments monitoring fluorophore absorbance at 254 nm, intact conjugate **2** elutes rapidly because its large size results in minimal interactions with column packing material. Any fragmentation of conjugate **2** would be visible as a secondary peak with significantly longer retention time, with free fluorogenic dye **1a** (t_R = 32.3 min) as reference. We found that conjugate **2** was stable in acid (even at 60 °C), growth medium, and cell lysates (Figures 2, S9, and S10). These data suggest that the cytosolic fluorescence (Figure 1) arises from intact conjugate **2**.

We sought to examine if there were any inherent structural differences in conjugate **2** relative to other dextrans that might

DOI: 10.1021/acs.bioconjchem.8b00198
Bioconjugate Chem. 2018, 29, 1942−1949

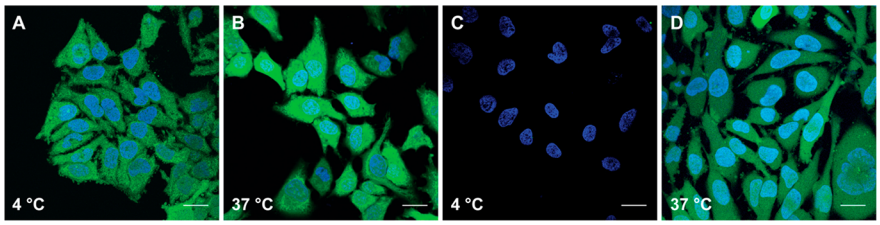

Figure 3. Confocal microscopy images showing the effect of temperature on the uptake of probe **1a** (5 μM; A and B) and conjugate **2**. (5 μM; C and D) by HeLa cells. Scale bars: 25 μm.

cause cell penetration. Physical characterization of dextrans typically entail determining their average hydrodynamic radius (which is correlated with molecular mass) and branching ratios.[2,32−,34] We were especially interested in deviations among the parent dextrans in our conjugates (**D1**−**D3**) as well as an unconjugated 100 kDa dextran (**D4**). We first determined the hydrodynamic radii, which agreed closely with standard parameters for dextrans.[33] Then, we verified that aggregation was not playing a significant role, as changes in concentration did not alter the hydrodynamic radius significantly (Figure S10).

The branching in a dextran can be calculated from ^{1}H NMR peak areas that correspond to α(1,6), α(1,4), and α(1,3) glycosidic linkages. We measured the branching ratios of all dextrans using glucose disaccharides with α(1,6), α(1,4), and α(1,3) linkages as standards. The frequency of α(1,4) branches between dextrans **D1** and **D2** varied by 3%, whereas dextran **D4** was branched half as frequently (Table S2, Figures S11A−H). The dextrans showed 2-fold differences in the frequency of rare α(1,3) branches, and no dextrans appeared to have detectable α(1,2) branches. Protein−carbohydrate interactions can be highly specific,[35] and additional studies are needed to identify causal relationships between structural variations and the unusual transport properties of dextran **D1**.

To better understand the transport process, we conducted mechanistic studies of the cellular entry of conjugate **2**. Lowering environmental temperature to 4 °C is known to inhibit active transport (e.g., endocytosis), which is energy-dependent.[36−38] At 4 °C, we observed no cellular uptake of conjugate **2**, indicating that its entry relies on active transport rather than passive diffusion (Figure 3C,D). These data are in agreement with previous work showing dextran uptake through a mixture of clathrin-mediated endocytosis and macropinocytosis,[25] both energy-dependent processes inhibited by low temperatures. In contrast, small-molecule probe **1a** diffused across the membrane and stained the cytosol similarly at 4 and 37 °C (Figure 3A,B).

Endocytic processes can largely be classified into three components—pinocytosis, phagocytosis, and receptor-mediated endocytosis.[8] Unlike the specific cargo−receptor interactions required for receptor-mediated endocytosis, pinocytosis entails the ingestion of solutes in a nonspecific manner. Competition assays titrating labeled fluorogenic dextran with unlabeled dextran provide a means to study the extent of reliance on receptor-mediated transport.[39] HeLa cells were incubated with a constant concentration of conjugate **2** while varying the unlabeled dextran, then imaged using confocal microscopy. Because the added unlabeled dextran does not contain a fluorophore, any loss of signal is directly proportional to lowered uptake of conjugate **2**. Quantification of the resulting cell images shows an exponential decay of the signal from conjugate **2** versus increasing concentrations of unlabeled dextran (Figure 4). The exponential (rather than linear) nature of the curve is diagnostic of a receptor-mediated process.[40] An

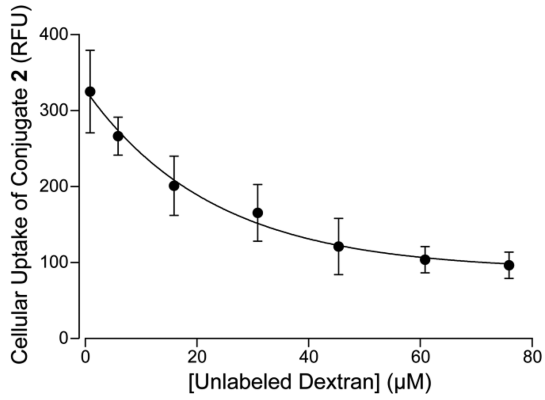

Figure 4. Graph showing the effect of increasing concentrations of unlabeled dextran on the uptake of conjugate **2** by live HeLa cells. Uptake was quantified by confocal microscopy after a 30 min incubation with conjugate **2** (5 μM) and unlabeled dextran (0−75 μM).

asymptotic basal level of uptake was observed, which can be attributed to the rate of nonspecific uptake via pinocytosis. Thus, the uptake of conjugate **2** occurs via a combination of receptor-mediated endocytosis and pinocytosis.

CONCLUSION

We prepared a monofunctionalized fluorogenic dextran, conjugate **2**, with improved imaging capabilities compared to previous polyfunctionalized dextran−fluorophore conjugates. Our initial intent was to use conjugate **2** as a fluorogenic tracker for endocytosis. Conjugate **2** is impervious to pH fluctuations, easy to synthesize, and most importantly avoids the complications associated with nonspecific polyfunctionalization. Remarkably, conjugate **2** engages in highly productive cellular transport into the cytosol. Although this renders conjugate **2** a poor tracker of endocytosis, the rapid and disperse uptake observed with conjugate **2** suggests monofunctionalized dextrans as a vehicle for cytosolic delivery. Structural characterization following degradation experiments show that the cellular environment and its enzymatic machinery do not degrade **2**. Variations in the branching ratios or surface differences of dextrans investigated could be responsible for various transport properties. Encouraged by the results of the cellular uptake studies, we are currently investigating the mechanism of uptake while exploring alternative cargos that could use monofunctionalized dextrans as a delivery system.

DOI: 10.1021/acs.bioconjchem.8b00198
Bioconjugate Chem. 2018, 29, 1942−1949

EXPERIMENTAL PROCEDURES

Materials. Monothiodextran (100 kDa, **D1**) was purchased in three batches (JZ134P62, JZ13JP91, and MOS0099) from Fina Biosolutions (Rockville, MD). Polyaminodextran (70 kDa, **D3**) and TAMRA−dextrans (70 kDa and 100 kDa) were from Thermo Fisher Scientific (Waltham, MA). Unfunctionalized dextran (100 kDa, **D4**) was from Sigma−Aldrich (St. Louis, MO). Pig liver esterase (PLE) was from Sigma−Aldrich. All other materials were from Sigma−Aldrich, Fischer Scientific (Hampton, NH), or Alfa Aesar (Haverhill MA), and were used without further purification.

HeLa, H460, and H1299 cell lines were from American Type Culture Collection (Manassas, VA) and were maintained according to recommended procedures. Dulbecco's Modified Eagle's Medium (DMEM), RPMI 1640 medium, fetal bovine serum (FBS), trypsin (0.25% w/v), OptiMEM, and Dulbecco's phosphate-buffered saline (PBS) were from Thermo Fisher Scientific. HeLa cells were grown in DMEM supplemented with FBS (10% v/v), penicillin (100 units/mL), and streptomycin (100 μg/mL). H460 and H1299 cells were grown in RPMI 1640 medium supplemented with FBS (10% v/v), penicillin (100 units/mL), and streptomycin (100 μg/mL). For all imaging experiments, 8-well microscopy slides from Ibidi (Madison, WI) were seeded with 10^5 cells/mL 24 h before use. All imaging experiments were performed in live cells without fixation. ImageJ was used for all image-processing, signal quantification, and colocalization measurements.[41] HeLa cell lysates were prepared by treating HeLa cells with M-PER mammalian protein extraction reagent from Thermo Fisher Scientific (1 mL per 10^7 cells) with and without the addition of protease inhibitor (Pierce Protease Inhibitor tablets). Lysates elicited fluorescence from probe **1a** immediately, indicative of enzymatic activity (data not shown).

General Procedures. Chemical reactions were monitored by thin-layer chromatography (TLC) with EMD 250 μm silica gel 60-F254 plates visualized by UV illumination or $KMnO_4$ stain. Flash chromatography was performed on a Biotage Isolera automated purification system using prepacked SNAP KP silica gel columns.

The phrase "concentrated under reduced pressure" refers to the removal of solvents and other volatile materials using a rotary evaporator at water aspirator pressure (<20 Torr) while maintaining the water-bath temperature of 40 °C. Residual solvent was removed from samples by the vacuum (<0.1 Torr) achieved by a mechanical belt-drive oil pump.

All procedures were performed at ambient temperature (~22 °C) and pressure (1.0 atm) unless noted otherwise.

Instrumentation. ^{1}H and ^{13}C NMR spectra were acquired on Bruker spectrometers at the National Magnetic Resonance Facility at Madison (NMRFAM) operating at 500 MHz for ^{1}H and 125 MHz for ^{13}C. Electrospray ionization (ESI) mass spectrometry was performed with a Thermo Scientific Q Exactive Plus instrument at the Mass Spectrometry Facility in the Department of Chemistry at the University of Wisconsin−Madison. Dynamic light scattering data were acquired with a Malvern Zetasizer Nano ZSP instrument at the Soft Materials Laboratory of the University of Wisconsin−Madison. Microscopy images were acquired with a Nikon A1R-Si+ confocal microscope (60× objective, GaAsP PMT detector, 405 nm/488 nm excitation laser), at the University of Wisconsin−Madison Biochemistry Optical Core.

Fluorescence data were acquired with a PTI QuantaMaster spectrofluorometer. Absorbance measurements were made with an Agilent Cary 60 UV−vis spectrophotometer. Thiol−ene conjugation reactions were performed with a Spectronics Spectrolinker XL-1500 UV cross-linker. Dextran purity was verified with a Shimadzu LC-20 HPLC equipped with a Vydac C4 peptide 214TP510 column.

Optical Spectroscopy. All fluorogenic probes and fluorescent molecules were dissolved in spectroscopic grade DMSO and stored as frozen stock solutions. For all measurements, DMSO stock solutions were diluted such that the DMSO concentration did not exceed 1% v/v.

UV−vis and Fluorescence Spectroscopy. Spectroscopy was performed using 1 cm path length, 4 mL quartz cuvettes or 1 cm path length, 1 mL quartz microcuvettes. Fluorescence spectroscopy was performed on solutions that were stirred with a magnetic stir bar.

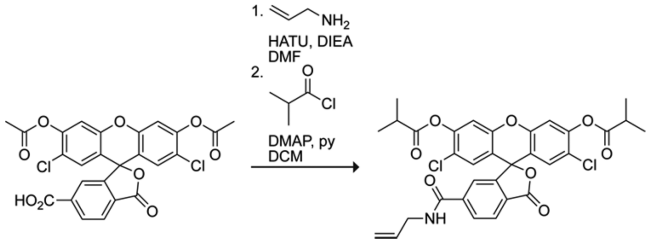

*Synthesis of 2′,7′-Dichloro-3′,6′-bis(isobutyryloxy)-3-oxo-3H-spiro[isobenzofuran-1,9′-xanthene]-6-carboxylic acid) (**1a**).* 3′,6′-Diacetyl-2′,7′-dichloro-6-carboxyfluorescein[42] (200 mg, 0.33 mmol), HATU (150 mg, 0.39 mmol), and diisopropylethylamine (144 μL, 0.83 mmol) were dissolved in DMF (2 mL). Allylamine (50 μL, 0.33 mmol) was added to the resulting solution, which was then stirred for 2 h. After concentration under reduced pressure, the residue was dissolved in EtOAc and washed with 1.0 M HCl and brine (3×), dried with $MgSO_4(s)$, and concentrated under reduced pressure. The residue was suspended in 10 mL of DCM. 4-Dimethylaminopyridine (4.0 mg, 33 μmol) and pyridine (106.4 μL, 1.32 mmol) were added to this suspension. Isobutyryl chloride (139 μL, 1.32 mmol) was added dropwise, and the resulting solution was stirred for 2 h. The mixture was diluted with water (50 mL) and DCM (50 mL). The organic phase was washed with saturated aqueous NH_4Cl and brine, dried with $MgSO_4(s)$, and concentrated under reduced pressure. Purification by column chromatography (0−60% v/v EtOAc in hexanes) on silica gel afforded the title compound as a white solid (146 mg, 62% yield). **^{1}H NMR** (500 MHz, $CDCl_3$, δ): 8.14 (d, J = 1.0 Hz, 2H), 7.51 (s, 1H), 7.13 (s, 2H), 6.84 (d, J = 3.5 Hz, 2H), 6.44 (t, J = 5.6 Hz, 1H), 5.89 (ddt, J = 16.1, 10.2, 6.0 Hz, 1H), 5.25 (dd, J = 17.1, 1.3 Hz, 1H), 5.18 (dd, J = 10.2, 1.2 Hz, 1H), 4.04 (tt, J = 5.9, 1.3 Hz, 2H), 2.89 (dt, J = 14.0, 7.0 Hz, 2H), 1.36 (dd, J = 7.0, 4.6 Hz, 13H). **^{13}C NMR** (125 MHz, $CDCl_3$, δ): 174.34, 167.80, 165.37, 152.60, 149.71, 148.93, 141.79, 133.36, 130.21, 129.09, 127.92, 126.28, 123.08, 122.32, 117.93, 116.81, 113.00, 80.72, 43.04, 34.27, 18.96. **HRMS−ESI** (m/z) calcd for $C_{32}H_{28}Cl_2NO_8$, 624.1187; found, 624.1178.

*Synthesis of 2′,7′-Dichloro-3′-(isobutyryloxy)-6′-((3-methylbut-1-en-2-yl)oxy)-3-oxo-3H-spiro[isobenzofuran-1,9′-xanthene]-6-carboxylic acid (**1b**).* 2′,7′-Dichloro-6-carboxyfluorescein[1] (200 mg, 0.45 mmol) was suspended in DCM. 4-Dimethylaminopyridine (5.5 mg, 45 μmol) and pyridine (144 μL, 1.8 mmol) were added to the suspension. Isobutyryl

DOI: 10.1021/acs.bioconjchem.8b00198
Bioconjugate Chem. 2018, 29, 1942−1949

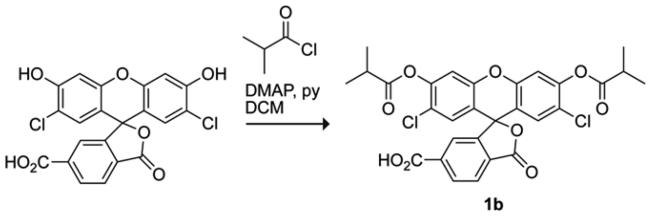

chloride (189 μL, 1.8 mmol) was added dropwise, and the resulting solution was stirred for 1 h. After dilution and extraction with DCM (3×), the combined organic extracts were washed with 1.0 M HCl and brine, dried with $MgSO_4(s)$, and concentrated under reduced pressure. Purification by column chromatography on silica gel (30−80% v/v EtOAc in DCM) afforded the title compound as a white solid (224 mg, 86% yield). **^{1}H NMR** (500 MHz, $CDCl_3$, δ): 8.40 (dd, J = 8.0, 1.1 Hz, 2H), 8.17 (d, J = 8.0 Hz, 2H), 7.90 (s, 2H), 7.17 (s, 4H), 6.85 (s, 4H), 2.89 (dt, J = 14.0, 7.0 Hz, 4H), 1.36 (dd, J = 7.0, 2.3 Hz, 21H). **^{13}C NMR** (125 MHz, $CDCl_3$, δ): 183.29, 174.00, 173.99, 169.22, 167.47, 152.15, 149.66, 148.82, 136.28, 132.36, 129.61, 128.71, 125.93, 125.76, 122.90, 116.61, 112.92, 80.86, 34.13, 18.82. **HRMS−ESI** (m/z): $[M + H]^+$ calcd for $C_{29}H_{23}Cl_2O_9$, 585.0714; found, 585.0712.

Ellman's Assay. Ellman's assay[43] was used to assess the concentration of free thiols in dextrans. The assays was performed in 0.10 M sodium phosphate buffer, pH 8.0, containing EDTA (1.0 mM) using ε = 14 150 M^{-1} cm^{-1} at 412 nm for reduced 5,5′-dithio-bis(2-nitrobenzoic acid).

Synthesis of Conjugate ***2***. Fluorogenic probe **1a** was conjugated to dextran **D1**, which has 0.82 (JZ134p62), 0.79 (JZ13JP91), or 0.31 (MOS0099) free thiols per dextran according to Ellman's assay, by a thiol−ene reaction.[44,45] The linker connecting the dextran and thiol in **D1** is located at the reducing end of the dextran and contains amide and ether moieties. All concentrations of conjugate **2** were measured as total dextran concentration (labeled and unlabeled), and all three batches showed identical same staining patterns and qualitative results. Quantitative fluorescence measurements were acquired with consistent batches of conjugate **2**.

Briefly, dextran **D1** (10 mg, 100 nmol) was dissolved in a solution of 200 μL of 0.20 M sodium acetate buffer, pH 4.0, 50 μL of acetonitrile, and 100 μL of DMSO. Glutathione (1.5 equiv), lithium phenyl-2,4,6-trimethylbenzoylphosphinate (LAP) initiator[44,45] (2.5 equiv), and probe **1a** (5 equiv) were added. The reaction mixture was irradiated with a 365 nm light source for 15 min. The resulting solution was diluted with 800 μL of PBS, transferred into a 10 kDa MWCO Slide-A-Lyzer MINI dialysis device from Thermo Fisher Scientific, and dialyzed against 1.0 L of PBS. After 2 h, the dialysis buffer was replaced, and dialysis was continued for an additional 8 h. TLC of conjugate **2** (60% v/v EtoAc in hexanes) showed a single baseline spot with no residual unconjugated probe **1a**. The average hydrodynamic radius (R_h = 6.3 nm) of the dextran was unchanged after conjugation. The absorbance spectrum of the dextran in aqueous 0.1 M NaOH (which hydrolyzes the isobutyryl esters) was indicative of >90% conjugation to free thiols (or an average of 0.29 fluorogenic moieties per dextran molecule). The purity of conjugate **2** from contaminating unconjugated probe **1a** was verified further by comparing HPLC traces of probe **1a**, dextran **D1**, and conjugate **2**, obtained using a linear gradient of B (10−95% v/v) over 45 min at a flow rate of 5 mL/min (A: H_2O containing 0.1% v/v TFA; B: acetonitrile containing 0.1% v/v TFA). Eluates were monitored at 254 nm.

Synthesis of Conjugate ***3a***. Thiol groups were installed on 70 kDa polyaminodextran. Briefly, the dextran (10 mg, 14 nmol) was reacted with succinimidyl 3-(2-pyridyldithio)-propionate (SDPD) from Thermo Fisher Scientific according to the manufacturer's instructions. The resulting polythiodextran (**D2**) was dissolved in sodium acetate buffer and conjugated with probe **1a** as described above for the synthesis of conjugate **2**. After irradiation, conjugate **3a** was dialyzed overnight against 1.0 L of PBS. Conjugate **3a** had an average of 11 fluorogenic moieties per dextran molecule.

Synthesis of Conjugate ***3b***. The NHS ester of probe **1b** was generated by stirring probe **1b** (10 μmol) with *N*-chlorosuccinimide (10 μmol) in DCM for 1 h, followed by removal of solvent under reduced pressure. The resulting NHS ester was used without further purification. 70 kDa polyaminodextran (10 mg, 14 nmol) was dissolved in 1.0 mL of PBS. To this solution was added 100 μL of a 30 mM solution of the NHS ester in DMSO. The resulting solution was stirred gently for 1 h, then dialyzed overnight against 1.0 L of PBS. Conjugate **3a** had an average of 9 fluorogenic moieties per dextran molecule.

Enzymatic Unmasking of Conjugate ***2***. PLE (168 kDa, ≥15 units/mg solid) was suspended in 10 mM HEPES−NaOH buffer at pH 7.3, and the resulting solution was diluted to appropriate concentrations before use in protein LoBind tubes from Eppendorf. Conjugate **2** (1 μM) in 10 mM HEPES−NaOH buffer, pH 7.3, was allowed to equilibrate with stirring in a cuvette for 5 min, after which PLE was added to final enzyme concentration of 9 nM. After stirring for 30 min, the absorption and emission spectra (λ_{ex} = 470 nm) were recorded.

Aggregation Assay. Solutions of dextrans were prepared in PBS at 1.0 mg/mL, 0.5 mg/mL, 0.25 mg/mL, 0.0125 mg/mL, and 0.00625 mg/mL, filtered through a 40 μm filter, and equilibrated for 30 min at 25 °C. The average hydrodynamic radius was measured by dynamic light scattering at 25 °C. Data were analyzed by the method of cumulants.[46]

Dextran Stability Assay. Solutions of dextrans were prepared in PBS at 1.0 mg/mL, filtered through a 40 μm filter, and equilibrated for 30 min at 25 °C. Solutions were then acidified to pH 0.4 by the addition of 1.0 M HCl, shaken thoroughly, and incubated for 15, 30, 45, or 60 min. The solutions were then neutralized by the addition of 1.0 M NaOH, and the average hydrodynamic radius was measured by dynamic light scattering at 25 °C.

Linker Stability Assay. The stability of the linker and dextran components in conjugate **2** was assessed by incubating conjugate **2** (10 μM) for 1 h in 1.0 mL of 1.0 M HCl, DMEM supplemented with fetal bovine serum (FBS, 10% v/v), penicillin (100 units/mL), and streptomycin (100 μg/mL), or HeLa cell lysate. The integrity of conjugate **2** was assessed by HPLC using a Vydac C4 peptide 214TP510 column as compared against probe **1a** eluted under the same conditions, which were an isocratic wash for 10 min followed by a linear gradient of B (10−95% v/v) over 45 min at 5 mL/min (A: H_2O containing 0.1% v/v TFA; B: acetonitrile containing 0.1% v/v TFA). Eluates were monitored at 254 nm, a wavelength that unconjugated dextran **D1** does not absorb significantly (Figure S1C). Note that the isobutyryl masking groups in conjugate **2** are cleaved by some of the incubation conditions, unveiling the parent dichlorofluorescein fluorophore conjugated to the dextran (see Scheme 1B). The difference in

DOI: 10.1021/acs.bioconjchem.8b00198
Bioconjugate Chem. 2018, 29, 1942−1949

polarity between unmasked and masked fluorophore does not significantly alter conjugate-retention time due to its large size excluding it from interaction with the resin. Although the presence or absence of the isobutyryl groups should materially affect retention times for dye-containing degradation fragments, no such degradation was observed in any of the tested incubation conditions.

Branching Assay. Solutions of dextrans **D1**−**D4**, kojibiose (α(1,2)), nigerose (α(1,3)), maltose (α(1,4)), and isomaltose (α(1,6)) were prepared in D_2O. ^{1}H NMR spectra of each solution were the recorded with 2048 scans. Disaccharide ^{1}H NMR spectra were used to establish the ^{1}H chemical shift of the proton attached to the anomeric carbon: α(1,3), 5.20−5.27 ppm; α(1,4), 5.30 ppm; α(1,6), 4.85 ppm; and α(1,2), 5.33 ppm. These chemical shifts were in close agreement with values reported previously.[6] Peaks in the ^{1}H NMR spectra of dextrans **D1**−**D4** that corresponded to these shifts were integrated, and the branching of the dextrans was calculated from the values of these integrals.

Time-Course Imaging. HeLa, H1299, or H460 cells in 8-well microscopy slides were incubated with Hoechst 33342 (2 μg/mL) for 15 min and washed. Dextran-conjugated probe (10 μM) was added to the well on stage, and images were acquired every 30 s. At each 30-s time point, data from the 408 and 488 nm excitation channels were acquired sequentially, with exposure time and excitation intensities selected to prevent saturation in images taken at the final time point. No wash steps were performed before or during imaging. The background-subtracted fluorescence signal and standard deviation for each the three time series were quantified with the program ImageJ.

4 °C Internalization Imaging. HeLa cells in 8-well microscopy slides were incubated at 4 °C with OptiMEM containing either conjugate **2** (10 μM) or small molecule **1a** (5 μM) for 20 min. The cells were counterstained with Hoechst 33342 (2 μg/mL) for 10 min at 4 °C, then washed thoroughly with OptiMEM at 4 °C to ensure complete removal of residual conjugate **2** or probe **1a** from the medium. Cells were then visualized with confocal microscopy at room temperature.

Pearson's Colocalization Coefficient. Pearson's colocalization coefficient was calculated for dextrans and Lysotracker or Hoechst 33342 by processing confocal images using an ImageJ plugin.[41] Regions of interest corresponding to individual cells were processed ($n \geq 20$), and the means and standard deviations for each experiment are listed in Table S1.

Competition Assay. HeLa cells in 8-well microscopy slides were incubated with conjugate **2** (5 μM) and dextran **D1** (0−75 μM) for 30 min. Cells were counterstained with Hoechst 33342 (2 μg/mL) for 10 min, washed, and visualized with confocal microscopy at room temperature. Overall uptake was calculated as the sum of cell area signal and compared. The resulting data was fit to a single exponential decay function using GraphPad Prism software with R^2 = 0.992, asymptote = 89.6 ± 10.6 RFU (95% CI, 47.1−114.9).

■ ASSOCIATED CONTENT

Supporting Information

The Supporting Information is available free of charge on the ACS Publications website at DOI: 10.1021/acs.bioconjchem.8b00198.

Pearson's correlation coefficients (r); Dextran branching as determined by ^{1}H NMR spectroscopy; Characterization of dextran conjugates; Confocal microscopy images; HPLC traces; ^{1}H NMR spectra (PDF)

■ AUTHOR INFORMATION

Corresponding Author

*E-mail: rtraines@mit.edu.

ORCID

Ronald T. Raines: 0000-0001-7164-1719

Author Contributions

#Wen Chyan and Henry R. Kilgore contributed equally.

Notes

The authors declare no competing financial interest.

■ ACKNOWLEDGMENTS

This work was supported by grant R01 GM044783 (NIH). W.C. was supported by an NSF Graduate Research Fellowship. NMRFAM was supported by Grant P41 GM103399 (NIH). The Mass Spectrometry Facility at the University of Wisconsin−Madison was supported by Grant S10 OD020022 (NIH). The Soft Materials Laboratory at the University of Wisconsin−Madison was supported by Grants S10 RR013790 (NIH) and BIR-9512577 (NSF).

■ REFERENCES

(1) Torino, M. I., de Valdez, G. F., and Mozzi, F. (2015) Biopolymers from lactic acid bacteria. Novel applications in foods and beverages. *Front. Microbiol. 6*, 1−16.

(2) Cheetham, N. W. H. (1990) Dextran structural details from high-field proton NMR spectroscopy. *Carbohydr. Polym. 14*, 149−158.

(3) Larsen, C. (1989) Dextran prodrugs—structure and stability in relation to therapeutic activity. *Adv. Drug Delivery Rev. 3*, 103−154.

(4) Varshosaz, J. (2012) Dextran conjugates in drug delivery. *Expert Opin. Drug Delivery 9*, 509−523.

(5) World Health Organization (2017) *WHO Model List of Essential Medicines, 20th list*, World Health Organization, Geneva, Switzerland.

(6) Auerbach, M., and Macdougall, I. (2017) The available intravenous iron formulations: History, efficacy, and toxicology. *Hemodial. Int. 21*, S83−S92.

(7) Li, Y.-L., Zhu, L., Liu, Z., Cheng, R., Meng, F. H., Cui, J.-H., Ji, S.-J., and Zhong, Z. Y. (2009) Reversibly stabilized multifunctional dextran nanoparticles efficiently deliver doxorubicin into the nuclei of cancer cells. *Angew. Chem., Int. Ed. 48*, 9914−9918.

(8) Marsh, M. (2001) *Endocytosis*, Oxford University Press, Oxford, UK.

(9) Oben, J. A., and Foreman, J. C. (1988) A simple quantitative fluorimetric assay of in vitro phagocytosis in human neutrophils. *J. Immunol. Methods 112*, 99−103.

(10) Deriy, L. V., Gomez, E. A., Zhang, G. P., Beacham, D. W., Hopson, J. A., Gallan, A. J., Shevchenko, P. D., Bindokas, V. P., and Nelson, D. J. (2009) Disease-causing mutations in the cystic fibrosis transmembrane conductance regulator determine the functional responses of alveolar macrophages. *J. Biol. Chem. 284*, 35926−35938.

(11) Barysch, S. V., Jahn, R., and Rizzoli, S. O. (2010) A fluorescence-based in vitro assay for investigating early endosome dynamics. *Nat. Protoc. 5*, 1127−1137.

(12) Sutherland, I. W. (1998) Novel and established applications of microbial polysaccharides. *Trends Biotechnol. 16*, 41−46.

(13) Kothari, D., Das, D., Patel, S., and Goyal, A. (2014) Dextran and Food Application, In *Polysaccharides* (Ramawat, K. G., and Merillon, J., Eds.) Springer.

(14) Yalpani, M., and Brooks, D. E. (1985) Selective Chemical Modifications of Dextran. *J. Polym. Sci., Polym. Chem. Ed. 23*, 1395−1405.

(15) Jeanes, A., and Wilham, C. A. (1950) Periodate oxidation of dextran. *J. Am. Chem. Soc. 72*, 2655−2657.

(16) Vocelle, D., Chesniak, O. M., Malefyt, A. P., Comiskey, G., Adu-Berchie, K., Smith, M. R., Chan, C., and Walton, S. P. (2016) Dextran functionalization enhances nanoparticle-mediated siRNA delivery and silencing. *Technology 4*, 42−54.
(17) Oliver, S., Thomas, D. S., Kavallaris, M., Vittorio, O., and Boyer, C. (2016) Efficient functionalisation of dextran-aldehyde with catechin: Potential applications in the treatment of cancer. *Polym. Chem. 7*, 2542−2552.
(18) https://assets.thermofisher.com/TFS-Assets/LSG/manuals/mp01800.pdf, accessed January 6, 2018.
(19) Hughes, L. D., Rawle, R. J., and Boxer, S. G. (2014) Choose your label wisely: Water-soluble fluorophores often interact with lipid bilayers. *PLoS One 9*, e87649.
(20) Maia, J., Carvalho, R. A., Coelho, J. F. J., Simoes, P. N., and Gil, M. H. (2011) Insight on the periodate oxidation of dextran and its structural vicissitudes. *Polymer 52*, 258−265.
(21) Chyan, W., Kilgore, H. R., Gold, B., and Raines, R. T. (2017) Electronic and steric optimization of fluorogenic probes for biomolecular imaging. *J. Org. Chem. 82*, 4297−4304.
(22) Lowe, A. B. (2010) Thiol−ene "click" reactions and recent applications in polymer and materials synthesis. *Polym. Chem. 1*, 17−36.
(23) Koniev, O., and Wagner, A. (2015) Developments and recent advancements in the field of endogenous amino acid selective bond forming reactions for bioconjugation. *Chem. Soc. Rev. 44*, 5743−5743.
(24) Oliver, J. M., Berlin, R. D., and Davis, B. H. (1984) Use of horseradish-peroxidase and fluorescent dextrans to study fluid pinocytosis in leukocytes. *Methods Enzymol. 108*, 336−347.
(25) Li, L., Wan, T., Wan, M., Liu, B., Cheng, R., and Zhang, R. Y. (2015) The effect of the size of fluorescent dextran on its endocytic pathway. *Cell Biol. Int. 39*, 531−539.
(26) Jiang, L. W., and Schindler, M. (1986) Chemical factors that influence nucleocytoplasmic transport—a fluorescence photobleaching study. *J. Cell Biol. 102*, 853−858.
(27) Schindler, M., and Jiang, L. W. (1986) Nuclear actin and myosin as control elements in nucleocytoplasmic transport. *J. Cell Biol. 102*, 859−862.
(28) Thorogate, R., and Torok, K. (2004) Ca^{2+}-dependent and -independent mechanisms of calmodulin nuclear translocation. *J. Cell Sci. 117*, 5923−5936.
(29) Tycko, B., and Maxfield, F. R. (1982) Rapid acidification of endocytic vesicles containing α_2-macroglobulin. *Cell 28*, 643−651.
(30) Yamashiro, D. J., Tycko, B., Fluss, S. R., and Maxfield, F. R. (1984) Segregation of transferrin to a mildly acidic (pH 6.5) para-Golgi compartment in the recycling pathway. *Cell 37*, 789.
(31) Magini, A., Polchi, A., Tancini, B., Urbanelli, L., Di Cristina, M., Mannucci, R., Nicoletti, I., and Emiliani, C. (2014) Methods to discriminate the distribution of acidic glycohydrolases between the endosomal−lysosomal systems and the plasma membrane. *Methods Enzymol. 534*, 25−45.
(32) Fahner, E. M., Grossmann, G. H., and Ebert, K. H. (1984) Elastic and quasielastic light scattering studies on the branching characteristics of dextrans. *Makromol. Chem. 185*, 2205−2212.
(33) Nordmeier, E., Xing, H., and Lechner, M.-D. (1993) Static and dynamic light scattering studies of dextran from *Leuconostoc mesenteroides* in the dilute region. *Makromol. Chem. 194*, 2923−2937.
(34) Ioan, C. E., Aberle, T., and Burchard, W. (2000) Structure properties of dextran. 2. dilute solution. *Macromolecules 33*, 5730−5739.
(35) Rillahan, C. D., and Paulson, J. C. (2011) Glycan microarrays for decoding the glycome. *Annu. Rev. Biochem. 80*, 797−823.
(36) O'Morchoe, C. C. C., Jones, W. R., III, Jarosz, H. M., O'Morchoe, P. J., and Fox, L. M. (1984) Temperature-dependence of protein-transport across lymphatic endothelium in vitro. *J. Cell Biol. 98*, 629−640.
(37) Mamdouh, Z., Giocondi, M. C., Laprade, R., and LeGrimellec, C. (1996) Temperature dependence of endocytosis in renal epithelial cells in culture. *Biochim. Biophys. Acta, Biomembr. 1282*, 171−173.
(38) Poirier, A., Lavé, T., Portmann, R., Brun, M. E., Senner, F., Kansy, M., Grimm, H. P., and Funk, C. (2008) Design, data analysis, and simulation of in vitro drug transport kinetic experiments using a mechanistic in vitro model. *Drug Metab. Dispos. 36*, 2434−2444.
(39) Zhang, D. S., Lee, H. F., Pettit, S. C., Zaro, J. L., Huang, N., and Shen, W. C. (2012) Characterization of transferrin receptor-mediated endocytosis and cellular iron delivery of recombinant human serum transferrin from rice (*Oryza sativa* L.). *BMC Biotechnol. 12*, 92.
(40) Attie, A. D., and Raines, R. T. (1995) Analysis of receptor−ligand interactions. *J. Chem. Educ. 72*, 119−124.
(41) French, A. P., Mills, S., Swarup, R., Bennett, M. J., and Pridmore, T. P. (2008) Colocalization of fluorescent markers in confocal microscope images of plant cells. *Nat. Protoc. 3*, 619−628.
(42) Woodroofe, C. C., Masalha, R., Barnes, K. R., Frederickson, C. J., and Lippard, S. J. (2004) Membrane-permeable and -impermeable sensors of the Zinpyr family and their application to imaging of hippocampal zinc in vivo. *Chem. Biol. 11*, 1659−1666.
(43) Ellman, G. L. (1959) Tissue sulfhydryl groups. *Arch. Biochem. Biophys. 82*, 70−77.
(44) Li, F. P., Allahverdi, A., Yang, R. L., Lua, G. B. J., Zhang, X. H., Cao, Y., Korolev, N., Nordenskiold, L., and Liu, C.-F. (2011) A direct method for site-specific protein acetylation. *Angew. Chem., Int. Ed. 50*, 9611−9614.
(45) Valkevich, E. M., Guenette, R. G., Sanchez, N. A., Chen, Y. C., Ge, Y., and Strieter, E. R. (2012) Forging isopeptide bonds using thiol−ene chemistry: Site-specific coupling of ubiquitin molecules for studying the activity of isopeptidases. *J. Am. Chem. Soc. 134*, 6916−6919.
(46) Koppel, D. E. (1972) Analysis of macromolecular polydispersity in intensity correlation spectroscopy: The method of cumulants. *J. Chem. Phys. 57*, 4814−4820.

DOI: 10.1021/acs.bioconjchem.8b00198
Bioconjugate Chem. 2018, 29, 1942−1949